Practical computation of axisymmetrical multifluid flows

Thomas Barberon, Philippe Helluy, Sandra Rouy

ISITV, Laboratoire ANAM/MNC, BP56, 83162 La Valette CEDEX. France.
helluy@univ-tln.fr

PRACTICAL COMPUTATION OF AXISYMMETRICAL MULTIFLUID FLOWS

THOMAS BARBERON, PHILIPPE HELLUY, SANDRA ROUY

Abstract. We adapt the Saurel-Abgrall front capturing finite volumes method for an industrial simulation of compressible multifluid flows. We then apply the method to the case of air-water flow in the cooling chamber of an axisymmetrical gas generator. We describe successively how to deal with exact and global Riemann solvers, pressure oscillations, unstructured meshes, axisymmetry, boundary conditions and overly restrictive CFL conditions. The resulting algorithm is efficient and robust.

1. Introduction

This work is devoted to the application of recent finite volumes schemes, and particularly the one proposed by Saurel and Abgrall in [24], to the simulation of an axisymmetrical multiphase flow in a complex geometry. Because of the complexity of the application, we have to specify or adapt the original Saurel-Abgrall idea to: global Riemann solver, unstructured meshes, axisymmetry, boundary conditions, multi time steps...

We base our simulation on an effective mathematical model for compressible multifluid flows and especially air-water flows. For our application, the pressure law for the air is a classical perfect gas law. Because we have in mind flows with high and low pressures, we have also to take into account the compressibility effects in water. In such applications, it is classical to observe *cavitation* zones in the liquid phase. Cavitation is a phenomenon that appears in a region of the flow where the pressure drops below the saturation pressure of water. In a first and very short stage, the liquid stays in a metastable state. It can also happen in this stage that the pressure becomes negative (it is then called a tension). In a second stage, a phase transition (vaporization) occurs. Thus the original two-phase flow, made of air and water, becomes a three-phase flow made of air, liquid and vapor. We restrict ourself to the two-phase case, where the phase transition has not started (or is not taken into account...). Then, as for the air, a pressure law which expresses the pressure of the water as a function of density and internal energy has to be supplied. We use a very simple generalization of the perfect gas law, the stiffened gas equation of state (see (2.1)), which allows negative values for the pressure.

Compressible single fluids have been extensively studied and the main difficulty here is the representation of the interface between the fluids. There are two main approaches for treating interfaces:

- One can favor the Lagrangian interpretation of the fluid equations. The interface then receives a particular treatment in the numerical method.

Key words and phrases. compressible multifluid, front capturing, nonconservative scheme, axisymmetry.

This work has been supported by a joint research grant DCN/ING Toulon & Région PACA..

This approach leads to the family of the *front-tracking methods*. We will not consider this kind of solution here.

- If the Eulerian point of view is preferred, the resulting scheme belongs to the family of the *front-capturing methods*. No special treatment is applied to the numerical cells that are crossed by the interface. We prefer the front-capturing methods because they are more general and easier to implement than the front-tracking methods.

A now classical and simple approach, proposed for example in [22], [19], is to locate the interface by means of the level-set of a function which is convected with the flow. In this approach only an advection equation has to be added to the classical compressible Euler model. One switches from one law (perfect gas) to the other (stiffened gas) according to the value of the level-set function. Because the stiffened gas law is a generalization of the perfect gas law, the level-set model is also equivalent, in our case, to a model where the two coefficients of the stiffened gas law are convected with the flow. The interface is then located by the discontinuities of the pressure law coefficients. Our model is finally made up of the Euler system (conservation of mass, momentum and energy, equations (2.3)), two additional transport equations (equations (2.5)) and the stiffened gas law (equation (2.1)). This multifluid model presents a supplementary transport equation when compared to the level-set model but it is generally easier to discretize.

Despite its simplicity and its mathematical perfection, this model leads to numerous numerical difficulties as shown in many works among which we can cite [1], [18], [19], [24], [3], [10], [23]... These difficulties have to be overcome before envisaging practical applications. Of greatest concern are the spurious pressure oscillations that appear near the material interface when the model is approximated by any conservative finite volumes scheme. The same kind of oscillations occurs in the simulation of mixtures of perfect gases [1] or across numerically diffused shear interfaces [5]. Actually, it appears that classical conservative schemes (such as Godunov's, Roe's, HLL, Rusanov's, etc.) suffer from a very slow convergence and a very bad precision on standard meshes when applied to the previous multifluid model. Mulder, Osher and Sethian did not mention this fact in [22] although they use in their work a classical conservative Roe scheme. Their trick to obtain acceptable numerical results is not detailed. Karni, in [18], points out this difficulty and proposes a simple hybrid scheme to remove the pressure oscillations. The idea is to solve the classical conservative equations far from the interface between the two fluids and a nonconservative pressure equation near the interface. The resulting nonconservative scheme, which is built in order to preserve constant pressure and velocity states, gives good results. But it is not clear, in the paper of Karni, whether the conservation error tends to zero with the step of the mesh. Indeed, as it is proved in the work of Hou and LeFloch [17], nonconservative schemes generally converge to wrong solutions. Then Abgrall in [2], Saurel and Abgrall in [24] propose a simpler approach based on the nonconservative convection of well chosen pressure law parameters. As in the work of Karni, the main idea in order to choose the good transported quantities, is to construct a scheme which preserves the moving contact discontinuities. In a one dimensional framework this is expressed by the fact that the pressure and the velocity should not change if they are constant at the first time step, but a numerical diffusion of the density is possible. The resulting scheme is quasi-conservative. More precisely, the numerical fluxes for mass, momentum and energy are conservative whereas the numerical fluxes for the gas law coefficients are not conservative. Hence, the resulting scheme allows slight mass transfers between the gas and the liquid. According to numerical experiments, this scheme seems to

be converging. This is not in contradiction with the previously cited result of Hou and LeFloch. Indeed, according to the Rankine-Hugoniot jump relations, the velocity of the flow and the gas law parameters cannot present a simultaneous jump. Thus the nonconservative products in the nonconservative transport equations are perfectly defined. Another interesting fix to the spurious oscillations is proposed by Fedkiw, Aslam, Merriman and Osher in [10], under the name of the Ghost Fluid Method. With the aid of a ghost fluid, these authors propose a nonconservative Godunov scheme where only one-fluid Riemann problems have to be solved. This method has been simplified by Abgrall and Karni in [3], under the name of the "Two-Flux Method". The Ghost Fluid and the Two-Flux methods are completely nonconservative at the interface. Numerical experiments (see [4]) seem to indicate that they converge, but there is still no complete theoretical justification of this "miracle".

Once the pressure oscillations have been corrected by an adequate scheme, still other difficulties remain. The remedies have more to do with numerical engineering than with mathematics but must be carefully assembled. In this way, we have to deal with axisymmetry, unstructured meshes, implementation of the Riemann solver, CFL condition...

This paper is thus organized as follows.

Following this Introduction, the second part is devoted to a presentation of the mathematical model. We describe its mathematical properties. The main feature is that the Riemann problem is globally well posed. This fact is important for the numerical simulation when a Godunov scheme is used. On the other hand the model allows negative values for the pressure. As we have already said, this can be justified in some physical configurations.

The third part begins with an exposition of the pressure oscillations that appear at the material interface in two-fluid simulations. We illustrate the pressure oscillations thanks to a simple test case. We recall the bases of the construction of the Saurel-Abgrall scheme. In the original Saurel and Abgrall paper [24], the construction is achieved with the help of the approximate Riemann solver of Rusanov. As detailed in [23], we use here instead an exact Riemann solver. In order to solve the convection of the pressure law coefficients, we use a nonconservative numerical flux based on the velocity of the contact in the Riemann solution between two cells. The Abgrall-Saurel reasoning is only valid for a multifluid flow where each fluid satisfies the stiffened gas law. For the sake of completeness, we also present another finite volumes scheme which preserves constant pressure-velocity states, and this for any gas law. This scheme is a Lagrange plus projection scheme. In the Lagrangian step, the contacts are perfectly resolved. The projection step is thus constructed in order to preserve this property. We propose to project the pressure back on the Eulerian grid instead of other conservative variables. The resulting scheme is valid for any pressure law and can be generalized to higher dimensions. This scheme is not conservative for the mass fraction it is thus precise only for moderate shocks. It is generally not convergent. For strong shocks a hybrid scheme should be used as in the papers of Karni [18], [19]: the idea would be to project the conservative variables near the shocks and the pressure near the contacts. Thus the Lagrange-projection scheme is not used in the sequel of the paper. It is slightly more diffusive and complex in its hybrid version than the Saurel-Abgrall scheme. Furthermore in

our application, the validity of the stiffened gas law is sufficient. The Lagrange-projection approach would be necessary to take into account the vaporization of the liquid in cavitation zones (see [4]).

The fourth part is devoted to an exposition of several practical difficulties that have to be solved before the application of the previous theory to an industrial problem:

- The first adaptation concerns the construction of a 2D axisymmetrical scheme based on the 1D scheme of Saurel and Abgrall that preserves moving contacts. It is not trivial to extend the idea of Saurel and Abgrall to higher dimensions. This is due to the fact that in higher dimensions the velocity is generally not continuous through a contact discontinuity - only the normal component is. Nkonga recently proposed a 2D scheme for resolving shear interfaces in [5]. His scheme perfectly resolves contact discontinuities aligned with the mesh, but because it is not conservative for the momentum, it is probably not convergent. In this paper we restrict ourselves to a scheme that preserves constant pressure-velocity states. First, we write a 3D Godunov scheme using the rotationnal invariance of the Euler equations, as usual. Some pressure law coefficients are convected in a nonconservative way, as in the Saurel-Abgrall scheme. Then we restrict this scheme to an axisymmetrical mesh. This leads to a 2D axisymmetrical scheme. The interest of this approach is to avoid complicated source terms that arise from the axisymmetrical Euler equations. It must be pointed out that in the literature many authors (as [25], [20], etc.) do not follow this (in our sense) correct approach and have to deal with singular source terms on the axis of rotation.
- The second necessary adaptation deals with the boundary conditions. We shall use in the application a classical treatment of the boundary conditions by defining artificial cells on the boundary. In order to define the physical values of the artificial cells, we follow the approach of partial Riemann problems as in the works of Dubois and LeFloch [9], [8].
- In our application, the geometry of the mesh is quite complex. This imposes the use of unstructured meshes. We thus have to develop a special technique of multiple time steps because the CFL condition given by the small cells is too restrictive. On each edge we define a local time step which is a power of two times the minimal time step. This local time step satisfies the CFL condition of the two neighboring cells. Then more time steps are performed on the small cells than on the big cells, with possible "rendez-vous" because the ratio of two different time steps is a power of two. The resulting scheme is stable, and the computation time is reduced by a significant factor.

In the fifth part we present numerical results obtained in the case of an axisymmetrical gas generator. As we have said before, the gas generator geometry is quite complex. Several kinds of boundary conditions have to be considered. Because of the presence of very small holes, the ratio between the biggest cell and the smallest cell in the mesh is of the order of 10. All these facts justify our previous approach. We are then able to present a complete simulation of this industrial system. According to preliminary measurements, our simulation gives, at least qualitatively, good results. More details are given in [23].

The sixth part is the conclusion of the paper.

We then end the paper with an appendix (seventh part) where some computations are detailed:

- First we perform classical computations concerning hyperbolicity and entropy. We also recall the mathematical equivalence of the conservative equations with the nonconservative form of Saurel-Abgrall. This fact would permit to prove a Lax-Wendroff convergence result for the Saurel-Abgrall scheme and thus presents some interest.
- Second, we prove that the Riemann problem for a two-fluid flow governed by a stiffened gas law is globally well posed. In the case of strong rarefaction waves, it is necessary to introduce negative pressures and/or vacuum regions. The proof uses standard arguments but we have not found it in the literature. The notations that we have to set are also useful for a rigorous definition of the boundary conditions that are described in part 4.

2. A two-fluids model for air-water flows

2.1. **Basic equations.** We are interested in the flow of a compressible continuous medium characterized by its density $\rho(t,x)$, its velocity $u(t,x)$, and its internal massic energy $\varepsilon(t,x)$. The time variable is denoted by t, the space variable is x, and for simplicity we present the model in one space dimension. The pressure $p(t,x)$ of the medium is expressed by a stiffened gas Equation Of State (EOS)

$$p = (\gamma - 1)\rho\varepsilon - \gamma\pi. \tag{2.1}$$

Because we are studying a flow of several fluids, the two parameters γ and π of the pressure law also depend on time and space

$$\gamma = \gamma(t,x) \quad \text{and} \quad \pi = \pi(t,x). \tag{2.2}$$

Conservation of mass, momentum and energy lead to the three Euler equations

$$\begin{aligned} \rho_t + (\rho u)_x &= 0, \\ (\rho u)_t + (\rho u^2 + p)_x &= 0, \\ (\rho E)_t + ((\rho E + p)u)_x &= 0, \end{aligned} \tag{2.3}$$

where E, the total massic energy, is defined by

$$E = \varepsilon + \frac{u^2}{2}. \tag{2.4}$$

On the other hand, the pressure law parameters are convected with the flow

$$\begin{aligned} \gamma_t + u\gamma_x &= 0, \\ \pi_t + u\pi_x &= 0. \end{aligned} \tag{2.5}$$

If the gas is supposed to be perfect and polytropic (this will always be the case in the sequel), we set $\gamma = \gamma_{\text{gas}}$ and $\pi = 0$. For the liquid, the stiffened gas EOS is still valid. It reads

$$p = (\gamma_{\text{liq}} - 1)\rho\varepsilon - \gamma_{\text{liq}}\pi_{\text{liq}}.$$

The constants γ_{liq} and π_{liq} are chosen in order to match physical measurements. Cocchi and Saurel in [7] have proposed the following values for γ_{liq} and π_{liq}

$$\begin{aligned} \gamma_{\text{liq}} &= 5.5, \\ \pi_{\text{liq}} &= 4900 \text{ bar}. \end{aligned} \tag{2.6}$$

These values are based on sound speed and shock speed measurements.

In this model, the interface between air and water can be located by the discontinuity of $\gamma(t,x)$ or $\pi(t,x)$. It must be pointed out that mathematically, the model is

perfectly equivalent to a level-set model (as the one of [22]). In the level-set model, equations (2.5) are replaced by the convection of a level-set function

$$\varphi_t + u\varphi_x = 0, \tag{2.7}$$

and the pressure law (2.1) by

$$p = (\gamma(\varphi) - 1)\rho\varepsilon - \gamma(\varphi)\pi(\varphi). \tag{2.8}$$

But it appears that numerically, it is not equivalent to discretize (2.3), (2.1), (2.5) or (2.3), (2.8), (2.7).

2.2. **Properties of the model.** Our system (2.3), (2.1), (2.5) can be expressed in the classical form of a system of conservation laws (the equivalence between the non-conservative form and the conservative form is rigorously proved in section 7: see remark 7.3)

$$W_t + F(W)_x = 0, \tag{2.9}$$

with

$$W = \begin{pmatrix} \rho \\ \rho u \\ \rho E \\ \rho\gamma \\ \rho\pi \end{pmatrix}, \quad F(W) = \begin{pmatrix} \rho u \\ \rho u^2 + p \\ (\rho E + p)u \\ \rho\gamma u \\ \rho\pi u \end{pmatrix},$$

and the pressure law (2.1).

If c is the sound speed associated with the pressure law (2.1), it verifies

$$c^2 = \gamma\frac{p+\pi}{\rho}. \tag{2.10}$$

The hyperbolicity of the system (2.9) then implies that

$$p + \pi \geq 0. \tag{2.11}$$

Thus, the model admits negative pressure in the water. Is this physically correct? Indeed, negative pressures can locally and briefly appear in a liquid, they should then be called *tensions*. But in the zone of negative pressures the liquid is in a metastable state and is subject to vaporization. This phenomenon is called *cavitation*. For a physical description of the cavitation, we refer to the book of Franc & *al* [11]. We have proposed recently a simple adaptation of the stiffened gas model to take into account cavitation (see [16]) but before the phase transition, or if the appearance of the tensions is very short, the stiffened gas law is still a good physical model. It must be pointed out that in our numerical simulations we will not use any special treatment when negative pressures occur. Some authors (as [10]) have proposed to correct the pressure by limiting it to zero when it is negative. This amounts to forgoing energy conservation and we think that it is worse from a physical point of view than negative pressures. It also causes additional numerical complications due to the kink in the limited gas law. For example, it is necessary to envisage a centered scheme on the cells where the pressure is limited.

There is another (mathematical) reason to keep this model. If one considers the Riemann problem associated to the system (2.9) and (2.1)

$$W_t + F(W)_x = 0, \tag{2.12}$$

$$W(0,x) = \begin{cases} W_l \text{ if } x < 0, \\ W_r \text{ if } x > 0. \end{cases} \tag{2.13}$$

The self-similar solution is noted

$$W(t,x) = R\left(\frac{x}{t}, W_l, W_r\right).$$

Then it can be shown that the solution is unique for any left and right states W_l and W_r satisfying the positivity of density and the hyperbolicity condition (2.11). The fact that the global Riemann problem can be uniquely solved is well known in the case of a monofluid flow. For example, it is solved in the book of Godunov [14] for the case of a one-fluid flow satisfying the stiffened gas law. In the case of strong rarefaction waves, the solution can present a region of vacuum in which

$$\begin{aligned} p &= -\pi_{\text{liq}}, \\ \rho &= 0. \end{aligned} \tag{2.14}$$

The solvability result can be extended to our model. For the sake of completeness, we prove it in the section 7. The global solvability of the Riemann problem is fundamental when one intends to use a Godunov type scheme, because it ensures the robustness of the resulting scheme. Another important property of the model is that it permits many equivalent formulations. Indeed, any function $f(\gamma, \pi)$ of γ and π is also convected with the flow. For example, the system (2.9), (2.1) is equivalent to

$$\begin{aligned} &\rho_t + (\rho u)_x = 0, \\ &(\rho u)_t + (\rho u^2 + p)_x = 0, \\ &(\rho E)_t + ((\rho E + p)u)_x = 0, \\ &(\rho/(\gamma-1))_t + (\rho u/(\gamma-1))_x = 0, \\ &(\rho\gamma\pi/(\gamma-1))_t + (\rho u\gamma\pi/(\gamma-1))_x = 0, \end{aligned} \tag{2.15}$$

with the stiffened gas law (2.1).

It is also equivalent to the following nonconservative form

$$\begin{aligned} &\rho_t + (\rho u)_x = 0, \\ &(\rho u)_t + (\rho u^2 + p)_x = 0, \\ &(\rho E)_t + ((\rho E + p)u)_x = 0, \\ &(1/(\gamma-1))_t + u(1/(\gamma-1))_x = 0, \\ &(\gamma\pi/(\gamma-1))_t + u(\gamma\pi/(\gamma-1))_x = 0, \end{aligned} \tag{2.16}$$

with the stiffened gas law (2.1).

The nonconservative form (2.16) plays a particular role among the other forms on the numerical point of view as we will see in the next section.

3. Nonconservative finite volumes approximation

This section is devoted to a short and simple presentation of the pressure oscillations phenomenon in the conservative Godunov schemes. It appears that for very simple one-dimensional test cases, the classical first order conservative Godunov scheme gives very bad results on every conservative form of the equations as (2.9) or (2.15). We first exhibit one of these test cases which is a simple Riemann problem.

Then, we present two fixes which permit to avoid the pressure oscillations at the interface:

- The first scheme is the Saurel-Abgrall scheme. The construction principle of this scheme is to require that it preserves the moving contact discontinuities. This condition leads to a nonconservative discretization of the transport of some pressure law coefficients. Let us recall that the conservative 1D Godunov scheme also preserves moving contact discontinuities in the case of a one-fluid flow. The nonconservative correction is only useful for multifluid

flows. The Saurel-Abgrall correction cannot be applied to other pressure laws than the stiffened gas law.

- The second scheme is a Lagrange plus remap scheme. This scheme works for any pressure laws but only for moderate shocks because it is not conservative for the mass fraction. It is based on the simple remark that during the Lagrangian step, the contact discontinuities are perfectly solved. In the remap step we thus project mass, momentum and energy as usual. We forget the mass fraction conservation and instead project the pressure. In this way, the pressure equilibrium of the two components is recovered.

These two schemes remove the pressure oscillation phenomenon and can be extended without difficulty to higher dimensions. The Saurel-Abgrall scheme is less diffusive than the Lagrange-plus-remap scheme. The Lagrange-plus-remap scheme is not convergent in its present form. It is possible to improve its precision for strong shocks by employing a hybrid version of the scheme: with the help of a level-set function, a conservative scheme is used far from the interface and the Lagrange-plus-remap approach near the contact. Hybrid schemes are described for example in [19] and [12]. Because we concentrate on the stiffened gas law, only the Saurel-Abgrall scheme is used in the sequel of the paper for the numerical experiments in two dimensions.

In this section, we restrict ourself to a Riemann problem initial condition. For the numerical experiments, we choose the following values

$$\begin{array}{llllll} \rho_l = 10 \text{ kg/m}^3 & u_l = 50 \text{ m/s} & p_l = 1.1 \times 10^5 \text{ Pa} & \gamma_l = 1.4 & \pi_l = 0, \\ \rho_r = 1 \text{ kg/m}^3 & u_r = 50 \text{ m/s} & p_r = 1 \times 10^5 \text{ Pa} & \gamma_r = 1.1 & \pi_r = 0. \end{array} \tag{3.1}$$

3.1. **Failure of the Godunov scheme.** In this section, we present numerical results obtained by a classical Godunov scheme. The approximated system is (2.15), but we would obtain very similar results for any other conservative formulation.

Consider a space step h and a time step τ. The discretization points are $x_i = ih, \quad i \in Z$. The cells C_i are centered on x_i, $C_i =]x_{i-1/2}, x_{i+1/2}[$. We look for an approximation of W in the cell C_i at time $t_n = n\tau$

$$W_i^n \simeq W(t_n, x), \quad x \in C_i.$$

A general conservative finite volumes scheme reads

$$W_i^{n+1} = W_i^n - \frac{\tau}{h}(F_{i+1/2}^n - F_{i-1/2}^n).$$

In the case of the Godunov scheme, the numerical flux is given by the resolution of a Riemann problem at each cell interface $x_{i+1/2}$ and takes the form

$$F_{i+1/2}^n = F(R(0^{+ \text{ or } -}, W_i^n, W_{i+1}^n)).$$

The initial conditions are (3.1). We plot only the pressure at time $t = 1$ ms. The study interval is $]0, L[$ with $L = 1$ m. The number of cells is fixed at $N = 400$ and the CFL number is 0.7. We observe pressure oscillations at the contact discontinuity (which is also the material interface between the two fluids). The results are in Figure 3.1.

3.2. **Nonconservative transport of the pressure law coefficients.** The conservative scheme gives very bad results and cannot be used for higher dimensional simulations. On the other hand, numerical experiments indicate that the situation is not better with another (approximate) Riemann solver. A second order MUSCL extension would slightly improve the results but it is not sufficient.

In order to improve the precision of the Godunov scheme, it is possible as proposed by Saurel and Abgrall in [24] to give up the last two conservation laws of the system (2.15) and replace them by a nonconservative transport equation to obtain

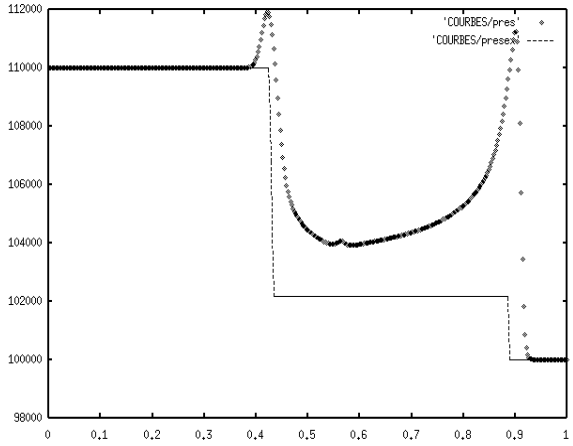

FIGURE 3.1. *Godunov scheme, pressure (line: exact; dots: numeric)*

(2.16). We show now why the special nonconservative form (2.16) plays a particular role for a finite volumes approximation. For this, let us consider a general conservative (for the mass, momentum and energy) upwind scheme. Suppose that we want to approximate a general moving contact discontinuity of constant velocity v and pressure p. We suppose that $v \gg 1$ and that the constant flow is supersonic. Then, because the speed $v > 0$, the upwind scheme reads

$$\rho_i^{n+1} = \rho_i^n - \frac{\tau}{h}\left((\rho u)_i^n - (\rho u)_{i-1}^n\right), \tag{3.2}$$

$$(\rho u)_i^{n+1} = (\rho u)_i^n - \frac{\tau}{h}\left((\rho u^2 + p)_i^n - (\rho u^2 + p)_{i-1}^n\right), \tag{3.3}$$

$$(\rho\varepsilon + \rho\frac{u^2}{2})_i^{n+1} = (\rho\varepsilon + \rho\frac{u^2}{2})_i^n - \frac{\tau}{h}\left((\rho\varepsilon u + \rho u\frac{u^2}{2} + pu)_i^n - (\rho\varepsilon u + \rho u\frac{u^2}{2} + pu)_{i-1}^n\right). \tag{3.4}$$

We now impose that the scheme preserves the moving contact discontinuities, i.e. that $u_i^{n+1} = u_i^n = v$ and $p_i^{n+1} = p_i^n = p$. We obtain

$$\rho_i^{n+1} = \rho_i^n - \frac{\tau}{h}\left((\rho v)_i^n - (\rho v)_{i-1}^n\right), \tag{3.5}$$

$$(\rho v)_i^{n+1} = (\rho v)_i^n - \frac{\tau}{h}\left((\rho v^2 + p)_i^n - (\rho v^2 + p)_{i-1}^n\right), \tag{3.6}$$

$$(\rho\varepsilon + \rho\frac{v^2}{2})_i^{n+1} = (\rho\varepsilon + \rho\frac{v^2}{2})_i^n - \frac{\tau}{h}\left((\rho\varepsilon v + \rho v\frac{v^2}{2} + pv)_i^n - (\rho\varepsilon v + \rho v\frac{v^2}{2} + pv)_{i-1}^n\right). \tag{3.7}$$

The two first equations reduce then to

$$\rho_i^{n+1} = \rho_i^n - \frac{\tau}{h}v\left(\rho_i^n - \rho_{i-1}^n\right), \tag{3.8}$$

while the last equation becomes

$$(\rho\varepsilon)_i^{n+1} = (\rho\varepsilon)_i^n - \frac{\tau}{h}v\left((\rho\varepsilon)_i^n - (\rho\varepsilon)_{i-1}^n\right). \tag{3.9}$$

But because $\rho\varepsilon = (p+\gamma\pi)/(\gamma-1)$, the only compatible approximations for γ and π are

$$\begin{aligned}
\left(\frac{1}{\gamma-1}\right)_i^{n+1} &= \left(\frac{1}{\gamma-1}\right)_i^{n} - \frac{\tau}{h}v\left(\left(\frac{1}{\gamma-1}\right)_i^{n} - \left(\frac{1}{\gamma-1}\right)_{i-1}^{n}\right), \\
\left(\frac{\gamma\pi}{\gamma-1}\right)_i^{n+1} &= \left(\frac{\gamma\pi}{\gamma-1}\right)_i^{n} - \frac{\tau}{h}v\left(\left(\frac{\gamma\pi}{\gamma-1}\right)_i^{n} - \left(\frac{\gamma\pi}{\gamma-1}\right)_{i-1}^{n}\right).
\end{aligned} \tag{3.10}$$

This is an upwind approximation of the transport equations

$$\begin{aligned}
(1/(\gamma-1))_t + v(1/(\gamma-1))_x = 0, \\
(\gamma\pi/(\gamma-1))_t + v(\gamma\pi/(\gamma-1))_x = 0.
\end{aligned} \tag{3.11}$$

Any scheme that reduces to (3.10) for constant velocity and pressure will then preserve moving contact discontinuities.

We propose now such a scheme. First, we define the interface values by the resolution of Riemann problems at the points $x_{i+1/2}$:

$$W_{i+1/2}^n = R(0, W_i^n, W_{i+1}^n).$$

For density, momentum and energy, the classical conservative approach is employed:

$$\begin{aligned}
\rho_i^{n+1} &= \rho_i^n - \frac{\tau}{h}((\rho u)_{i+1/2}^n - (\rho u)_{i-1/2}^n), \\
(\rho u)_i^{n+1} &= (\rho u)_i^n - \frac{\tau}{h}((\rho u^2+p)_{i+1/2}^n - (\rho u^2+p)_{i-1/2}^n), \\
(\rho E)_i^{n+1} &= (\rho E)_i^n - \frac{\tau}{h}\left(((\rho E+p)u)_{i+1/2}^n - ((\rho E+p)u)_{i-1/2}^n\right).
\end{aligned} \tag{3.12}$$

On the other hand, an upwind nonconservative scheme is used for the last two equations of (2.16). This nonconservative scheme is based on the contact discontinuity velocity of the Riemann problems solved at the points $(x_{i+1/2})$. It reads

$$\alpha_i^{n+1} = \alpha_i^n - \frac{\tau}{h}(\min(u_{i+1/2}^n, 0)(\alpha_{i+1}^n - \alpha_i^n) + \max(u_{i-1/2}^n, 0)(\alpha_i^n - \alpha_{i-1}^n)), \tag{3.13}$$

where the quantity α is $1/(\gamma-1)$ or $\gamma\pi/(\gamma-1)$. This choice is slightly different from the one of Saurel and Abgrall in [24] which is based on the approximate Riemann solver of Rusanov. It is easy to check that the scheme (3.13) reduces to (3.10) for constant velocity and pressure states.

With the scheme (3.12), (3.13), the results on the same test case as above are given in Figure 3.2. There is an evident improvement.

Unfortunately, the previous reasoning cannot be extended to a pressure law which is not linear with respect to $\rho\varepsilon$. To be more general we thus present in the next paragraph a general approach to deal with non-linear pressure laws.

3.3. **A Lagrange plus remap scheme for two-fluids flow.** In this section we describe the results obtained with a Lagrange plus remap scheme. In order to have a clear description of the scheme, we will recall the bases of the Lagrange scheme construction (see [13]).

Notations. We wish to approximate the system of conservation laws.

$$W_t + F(W)_x = 0. \tag{3.14}$$

For this purpose, we consider an increasing sequence of instants $(t^n)_{n\in\mathrm{N}}$ and a sequence of subdivisions of space defined by the points $(x_i^n)_{i\in\mathrm{Z},n\in\mathrm{N}}$ which satisfy

$$\forall i \in \mathrm{Z},\ \forall n \in \mathrm{N}, \quad x_i^n < x_{i+1}^n.$$

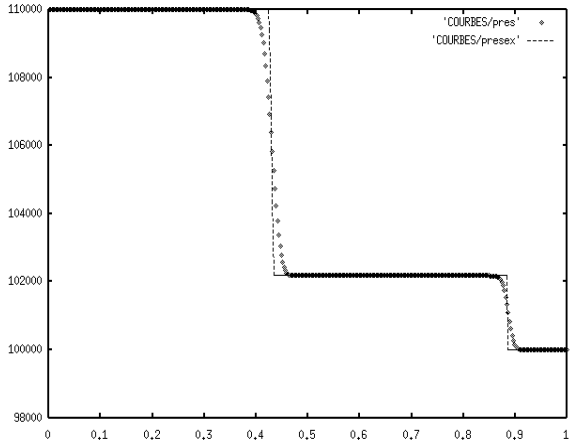

FIGURE 3.2. *Saurel-Abgrall scheme, pressure (line: exact; dots: numeric)*

The point x_i^n will be the center of the cell C_i^n. In order to define properly these cells, we thus introduce the boundary points

$$x_{i+1/2}^n = \frac{x_i^n + x_{i+1}^n}{2}.$$

The cell C_i^n is then

$$C_i^n = \Big] x_{i-1/2}^n, x_{i+1/2}^n \Big[.$$

The time steps are

$$\tau^n = t^{n+1} - t^n.$$

The lengths of the cells are

$$h_i^n = x_{i+1/2}^n - x_{i-1/2}^n.$$

In a Lagrange scheme, the cell boundaries move between the time step t^n and t^{n+1} with the velocity $u_{i+1/2}^n$. Thus,

$$x_{i+1/2}^{n+1} = x_{i+1/2}^n + \tau^n u_{i+1/2}^n.$$

A CFL condition has to be provided in order that the points $x_{i+1/2}^{n+1}$ stay ordered.

Scheme construction. We suppose that at time t^n we know an approximation W^n of the exact solution W. The approximation is supposed to be constant in each cell

$$W(t^n, x) \simeq W^n(x) = W_i^n, \quad x \in C_i^n.$$

We then compute exactly for a time τ^n, the entropic solution of

$$\begin{array}{l} V_t + F(V)_x = 0, \\ V(0,x) = W^n(x), \quad x \in \mathrm{R}. \end{array}$$

This exact resolution is possible under a CFL condition.

The new approximation of W at time t^{n+1} is then defined as the mean value of the exact solution in the new cells

$$W_i^{n+1} = \frac{1}{h_i^{n+1}} \int_{C_i^{n+1}} V(\tau_n, x) dx.$$

The Riemann problem reads

$$\begin{array}{l} U_t + F(U)_x = 0, \\ U(0,x) = \left\{ \begin{array}{ll} W_l & x < 0, \\ W_r & x > 0. \end{array} \right. \end{array}$$

The solution is self-similar; as before it is noted

$$R(x/t, W_l, W_r) = U(t,x).$$

In order to have a simpler expression of the scheme, we express the conservation law in the space-time trapezoid Q whose parallel sides are C_i^n and C_i^{n+1}.

$$0 = \int_Q (W_t + F(W)_x) dx \wedge dt = \int_{\partial Q} (F(W)dt - W dx).$$

The contour integral in the right hand side is the sum of four contributions (bottom, top, right and left)

$$\begin{array}{c} \int_{\partial Q} (F(W)dt - W dx) = \int_{C_i^n} -W_i^n dx \\ + \int_{C_i^{n+1}} W_i^{n+1} dx \\ + \int_{t=0}^{t=\tau^n} \left(F(R(u^n_{i+1/2}, W_i^n, W_{i+1}^n)) - R(u^n_{i+1/2}, W_i^n, W_{i+1}^n) u^n_{i+1/2} \right) dt \\ - \int_{t=0}^{t=\tau^n} \left(F(R(u^n_{i-1/2}, W_{i-1}^n, W_i^n)) - R(u^n_{i-1/2}, W_{i-1}^n, W_i^n) u^n_{i-1/2} \right) dt. \end{array}$$

This gives

$$\begin{array}{c} 0 = h_i^{n+1} W_i^{n+1} - h_i^n W_i^n \\ +\tau_n \left(F(R(u^n_{i+1/2}, W_i^n, W_{i+1}^n)) - R(u^n_{i+1/2}, W_i^n, W_{i+1}^n) u^n_{i+1/2} \right) \\ -\tau_n \left(F(R(u^n_{i-1/2}, W_{i-1}^n, W_i^n)) - R(u^n_{i-1/2}, W_{i-1}^n, W_i^n) u^n_{i-1/2} \right). \end{array} \tag{3.15}$$

When the velocities at the cell boundaries $u^n_{i+1/2}$ are zero, the scheme reduces to the classical Godunov scheme. Another important case is when the velocity $u^n_{i+1/2}$ is equal to the contact discontinuity velocity of the Riemann problem between the cells C_i^n and C_{i+1}. With this choice, a moving contact is perfectly resolved. The problem is now to come back properly from the Lagrangian grid $\left(C_i^{n+1}\right)$ to the Eulerian grid (C_i^n). This is the goal of the remap step.

Remap step. Let us first describe the remap step of the classical Lagrange and projection scheme. Actually, the formula (3.15) defines a value $W_i^{n+1/2}$ of the conservative variables in the new cells C_i^{n+1}. This value has now to be averaged on the old cells C_i^n. This is usually done with the formula

$$\begin{array}{c} W_i^{n+1} = \frac{\tau}{h} \max(u^n_{i-1/2}, 0) W_{i-1}^{n+1/2} - \frac{\tau}{h} \min(u^n_{i+1/2}, 0) W_{i+1}^{n+1/2} + \\ (1 - \frac{\tau}{h} \max(u^n_{i-1/2}, 0) + \frac{\tau}{h} \min(u^n_{i+1/2}, 0)) W_i^{n+1/2}. \end{array}$$

Our scheme is then a very simple correction of the Lagrange-projection scheme. The projection is the same for density, momentum and energy. But instead of projecting the last conservative variable $\rho/(\gamma - 1)$, we project the pressure according to the formula

$$\begin{array}{c} p_i^{n+1} = \frac{\tau}{h} \max(u^n_{i-1/2}, 0) p_{i-1}^{n+1/2} - \frac{\tau}{h} \min(u^n_{i+1/2}, 0) p_{i+1}^{n+1/2} + \\ (1 - \frac{\tau}{h} \max(u^n_{i-1/2}, 0) + \frac{\tau}{h} \min(u^n_{i+1/2}, 0)) p_i^{n+1/2}. \end{array}$$

It is then possible to compute γ_i^{n+1} thanks to the pressure law (according to (3.1), the value of π is indeed 0). In test cases where $\pi \neq 0$ another quantity has to be projected in order to recover γ_i^{n+1} and π_i^{n+1}. It could be for example the temperature.

Numerical results. With the Lagrange-projection scheme, we obtain the results in Figure 3.3. They are comparable to the results of the Saurel-Abgrall approach but are a little bit more diffusive. This extra diffusion is classical and is of course due to the double projection: Godunov averaging and remap averaging. This method can be applied though to more general pressure laws.

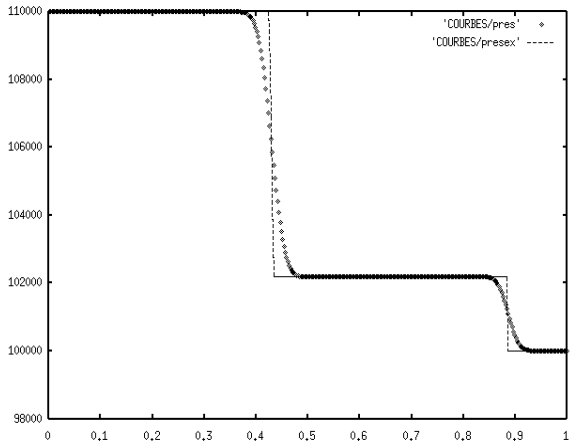

FIGURE 3.3. *Lagrange and remap scheme, pressure (line: exact; dots: numeric)*

4. Axisymmetrical extension of the Godunov scheme

4.1. **Scheme construction and properties.** In this paragraph, we present the extension of scheme (3.12, 3.13) to an industrial axisymmetrical case. We will first describe a 3D scheme without source term for which stability under a CFL condition is well established. Then, using special meshes with a rotational invariance we will deduce the 2D axisymmetrical scheme keeping the same CFL stability condition. This 2D scheme presents a pressure source term that is thus handled explicitly.

Consider a mesh of a 2D open set $\Omega \subset R^2$, that is to say a family of open sets $(\Omega_k)_{1\leq k\leq N}$ satisfying

$$\overline{\Omega} = \bigcup_k \overline{\Omega_k},$$
$$i \neq j \Rightarrow \Omega_i \cap \Omega_j = \oslash.$$

We suppose also that $(x,z) \in \Omega \Rightarrow x > 0$. A 3D mesh can be generated by a rotation of Ω around the axis $x = y = 0$ in a referential (x,y,z). Introducing cylindrical coordinates (r,ϕ,z):

$$\begin{aligned} x &= r\cos\phi, \\ y &= r\sin\phi, \\ z &= z, \end{aligned}$$

we define the family $(Q_{k,l})$, $1 \leq k \leq N$, $0 \leq l \leq P-1$ by

$$Q_{k,l} = \left\{ (x,y,z) \in R^3, (r,z) \in \Omega_k \text{ and } \phi \in]\frac{2(l-1/2)\pi}{P}, \frac{2(l+1/2)\pi}{P}[\right\}.$$

In order to simply define the 3D scheme, we will slightly change the notations. The velocity $\overrightarrow{u}$ is now a vector $\overrightarrow{u} = (u^1, u^2, u^3)^T$. W will be now the vector of conservative variables $(\rho, \rho\overrightarrow{u}, \rho E)^T$, with $E = \varepsilon + \frac{\overrightarrow{u}\cdot\overrightarrow{u}}{2}$. The vector of nonconservative

variables is denoted by $Y = (\alpha, \beta)^T$ with

$$\alpha = \frac{1}{\gamma - 1}, \quad \beta = \frac{\gamma \pi}{\gamma - 1}. \tag{4.1}$$

We define also a mixed vector as $V = (W, Y)^T$.

In 3D, the Euler equations read (I_d is the identity matrix of size $d \times d$)

$$\begin{aligned} \rho_t + \nabla \cdot (\rho \overrightarrow{u}) &= 0, \\ (\rho \overrightarrow{u})_t + \nabla \cdot (\rho \overrightarrow{u} \otimes \overrightarrow{u} + p I_3) &= 0, \\ (\rho E)_t + \nabla \cdot ((\rho E + p) \overrightarrow{u}) &= 0. \end{aligned}$$

Introducing the three fluxes:

$$\begin{aligned} G^1(W) &= (\rho u^1, \rho u^1 u^1 + p, \rho u^1 u^2, \rho u^1 u^3, (\rho E + p) u^1), \\ G^2(W) &= (\rho u^2, \rho u^2 u^1, \rho u^2 u^2 + p, \rho u^2 u^3, (\rho E + p) u^2), \\ G^3(W) &= (\rho u^3, \rho u^3 u^1, \rho u^3 u^2, \rho u^3 u^3 + p, (\rho E + p) u^3), \end{aligned}$$

and the vector flux $G = (G^1, G^2, G^3)^T$, the conservative equations can also be written

$$W_t + \nabla \cdot G(W) = 0.$$

Whereas for the nonconservative variables α and β, the equations are

$$Y_t + \overrightarrow{u} \cdot \nabla Y = 0,$$

and the pressure law is still the stiffened gas law which becomes

$$p = \frac{1}{\alpha} \rho \varepsilon - \frac{\beta}{\alpha}. \tag{4.2}$$

Now, a 3D scheme reads

$$\int_{Q_{k,l}} V_{k,l}^{n+1} - V_{k,l}^n + \tau \int_{\partial Q_{k,l}} F(V_{k,l}^n, V_{k',l'}^n, \nu) = 0,$$

where $V_{k,l}^n$ is the approximation of V in $\Omega_{k,l}$ at time t_n, ν is the outward normal vector to $Q_{k,l}$ on $\partial Q_{k,l}$ and $Q_{k',l'}$ denotes the neighbors of $Q_{k,l}$ along its boundary. The quantity $F(\cdot, \cdot, \nu)$ is the numerical flux that we will now precisely define. The definition of the numerical flux is based on the rotational invariance of the Euler equations. This is very classical (see [13]). The only originality is the special treatment of the nonconservative variables.

First, a unit vector $\nu = (\nu^1, \nu^2, \nu^3)^T$ is given. ν can also be written as $\nu = (\cos\phi \sin\theta, \sin\phi \sin\theta, \cos\theta)$. We define then the rotation matrix

$$M(\nu) = \begin{bmatrix} \cos(\phi)\sin(\theta) & \sin(\phi)\sin(\theta) & \cos(\theta) \\ -\sin(\phi) & \cos(\phi) & 0 \\ -\cos(\phi)\cos(\theta) & -\sin(\phi)\cos(\theta) & \sin(\theta) \end{bmatrix},$$

which satisfies $M(\nu)\nu = (1, 0, 0)^T$, and

$$N(\nu) = \begin{bmatrix} 1 & & 0 \\ & M(\nu) & \\ 0 & & I_3 \end{bmatrix}.$$

Consider now two states V_a and V_b. In order to compute $F(V_a, V_b, \nu)$, several steps are performed:

(1) Two rotated states are defined by $\widetilde{V}_a = M(\nu) V_a$ and $\widetilde{V}_b = M(\nu) V_b$.

(2) The following augmented Riemann problem in the normal direction is then solved

$$\widetilde{W}_t + G^1(\widetilde{W})_x = 0,$$
$$\widetilde{Y}_t + \widetilde{u^1}\widetilde{Y}_x = 0,$$
$$\widetilde{V}(0,x) = \begin{cases} \widetilde{V}_a \text{ if } x < 0, \\ \widetilde{V}_b \text{ if } x > 0, \end{cases}$$

and the solution of this Riemann problem at $x/t = 0$ is denoted by $\widetilde{V^*}$.

(3) An interface state is recovered by the inverse rotation $V^* = M(\nu)^{-1}\widetilde{V^*}$.

(4) The numerical flux is then set to

$$F(V_a, V_b, \nu) = (G(W^*)\cdot\nu, \min(u^*\cdot\nu, 0)(Y_b^* - Y_a^*))^T. \tag{4.3}$$

It must be noted that *this numerical flux is nonconservative on the Y variables*, as in the Saurel-Abgrall scheme that we presented in 1D cases. It can be proved, as in the 1D case, that the resulting scheme preserves constant pressure and velocity states.

In our case the scheme will reduce to a 2D one thanks to several simplifications.

First, thanks to the rotation matrix $J(\phi) = N(\cos\phi, -\sin\phi, 0)$ the axisymmetry condition reads

$$V_{k,l'}^n = J(\frac{2(l'-l)\pi}{P})V_{k,l}^n\,.$$

Thus, the velocity vector can be written $\overrightarrow{u}_{k,l} = (u_k\cos(\frac{2l\pi}{P}), u_k\sin(\frac{2l\pi}{P}), v_k)^T$ and the other variables do not depend on l. In this way, the scheme has only to be written on the cells $Q_{k,0}$:

$$\int_{Q_{k,0}}(V_{k,0}^{n+1} - V_{k,0}^n) + \tau\int_{\partial Q_{k,0}} F(V_{k,0}^n, J\left(\frac{2l'\pi}{P}\right)V_{k',0}^n, \nu) = 0.$$

Denoting $V_{k,0}$ by V_k, this scheme then becomes

$$\int_{\Omega_k}(V_k^{n+1} - V_k^n)r dr\,dz + \tau\int_{\partial\Omega_k} F(V_k^n, V_{k'}^n, \nu)r d\sigma +$$

$$\frac{\tau P}{2\pi}\left(\int_{\Omega_k} F(V_{k,0}^n, J\left(\frac{2\pi}{P}\right)V_{k,0}^n, \nu)r dr\,dz + \int_{\Omega_k} F(V_{k,0}^n, J\left(\frac{-2\pi}{P}\right)V_{k,0}^n, \nu)r dr\right) = 0.$$

It is then natural to let P tend to ∞. In the Riemann problems of the two last integrals only symmetric rarefaction waves occur. Thus those two terms reduce to a pressure term

$$\int_{\Omega_k}(V_k^{n+1} - V_k^n)r dr + \tau\int_{\partial\Omega_k} F(V_k^n, V_{k'}^n, \nu)r d\sigma - \tau\int_{\Omega_k}(0, p_k^n, 0\cdots 0)^T r dr = 0. \tag{4.4}$$

We recover, of course, an approximation of the axisymmetrical equations, namely

$$\begin{aligned}
(\rho r)_t + (\rho u r)_x + (\rho v r)_z &= 0,\\
(\rho u r)_t + (\rho u^2 r + pr)_x + (\rho u v r)_z &= pr,\\
(\rho u r)_t + (\rho v u r)_x + (\rho v^2 r + pr)_z &= 0,\\
(\rho E r)_t + ((\rho E + p)u r)_x + ((\rho E + p)v r)_z &= 0,\\
\alpha_t + u\alpha_x + v\alpha_z &= 0,\\
\beta_t + u\beta_x + v\beta_z &= 0.
\end{aligned}$$

One advantage of this approach is that the pressure source term can be handled explicitly without modifying the 3D CFL condition. We have also avoided axisymmetrical source terms which are singular on the axis of rotation. Finally, the resulting scheme preserves constant pressure and velocity states. The construction

of a 2D scheme that preserves contact discontinuities with discontinuous tangential velocity is proposed in Nkonga [5].

4.2. **Boundary conditions.** For a boundary cell Ω_k, an artificial value $V_{k'}^n$ has to be defined for the part of $\partial\Omega_k$ that meets the boundary. For simplicity, suppose that the normal vector is $\nu = (1, 0)$. We index by (i) (as "inside") the components of V_k^n and by (o) (as "outside") the (unknown) components of $V_{k'}^n$. Several boundary conditions can then be used:

- "Supersonic" inlet:
$$V_o = \text{given state.}$$
- "Supersonic" outlet:
$$V_o = V_i.$$
- Pressure imposed ("subsonic" outlet). The outside state with pressure p_o is linked to the inside state by a one-wave (shock or rarefaction). With the notations of §7.2, we find
$$\begin{aligned} \rho_o &= 1/H_i(p_o), \\ u_o &= u_i - X_i(p_o), \\ v_o &= v_i, \\ \alpha_o &= \alpha_i, \\ \beta_o &= \beta_i. \end{aligned}$$
- Pressure and density imposed ("subsonic" inlet). Pressure p_o and density ρ_o of the outside state are given. The nature of the outside state (α_o, β_o) and the tangential velocity (v_o) are also supposed to be known. Here, the outside state is linked to the inside state by a one-wave (shock or rarefaction) and a contact discontinuity. This permits to compute the unknown normal velocity
$$u_o = u_i - X_i(p_o).$$
- Mirror state. This boundary condition is used at a solid boundary. All the components of the state W_o are the same as those of state W_i but the normal velocity
$$u_o = -u_i.$$

It is important here to point out that the terminology "subsonic" or "supersonic" has nothing to do with the true nature of the flow at the boundary. It is only linked to what is expected when $W_o \simeq W_i$. Indeed, we can imagine imposing a "supersonic" inlet boundary condition and observing, at this boundary a supersonic outflow! The resolution of a Riemann problem ensures that the redundant information will be forgotten, if necessary. For more details about this technique, we refer to Dubois and his theory of partial Riemann problems [8].

4.3. **Optimisation of the CFL number.** An important constraint in any finite volumes scheme is the Courant-Friedrichs-Lewy condition. It expresses that, for any finite volume Ω_k the time step τ must verify

$$\tau < \frac{\text{surf}(\Omega_k)}{\text{length}(\partial\Omega_k)V^*} \quad , \tag{4.5}$$

where V^* is the maximal wave speed in the solution of all the Riemann problems at the cell interfaces. For a classical Godunov scheme on an unstructured mesh, it is proved in [6], that the CFL condition (4.5) implies the positivity of the scheme (the density remains >0) and the fact that it is entropic for any Lax entropy. We assume that this is still true for the Saurel-Abgrall scheme. In the case where large and small cells are mixed, the CFL condition on the small cells imposes the

global CFL condition. The mixing of large and small cells can be imposed by the geometry (an example is given below) and not necessarily by a required precision of the computation. In order to reduce the computational cost it is possible to use several time steps, a small one for the small cells and a bigger one for the big cells. Then, several time steps are performed on the small cells and less time steps are performed on the big cells. The time reduction of the computation can be significant.

The time marching algorithm can be formalized as follow.

First, in a initialization procedure, an ideal time step is computed for each cell Ω_k. Let δ be the desired CFL number (for example $\delta = 0.7$). The local time step is defined by

$$\tau_k = \delta \frac{\text{surf}(\Omega_k)}{\text{length}(\partial\Omega_k) V^*} \quad . \tag{4.6}$$

The maximal time step in the mesh is noted $\tau_{\max}$. In the same way, the minimal time step is $\tau_{\min}$. Let n_0 be the smallest integer such that $2^{n_0+1}\tau_{\min} > \tau_{\max}$ We will then say that the cell Ω_k has a *CFL level* of j if

$$2^{j-1}\tau_{\min} \leq \tau_k < 2^j \tau_{\min}. \tag{4.7}$$

Thus a CFL level of 1 corresponds to the smallest cells and a CFL level of n_0 corresponds to the biggest cells. We define also a CFL level for the edges. An edge E_l has a CFL level which is the smallest CFL level of its two neighboring cells. In order to advance by a global time step $2^{n_0}\tau_{\min}$, the algorithm is:

- for all integer $j = 1 \ldots n_0$ do
  - for all edges of CFL level $\leq j$ do
    - compute the flux
    - distribute it to the two neighboring cells
  - enddo
  - *update only the cells of level* $\leq j$
- enddo

In this way, the scheme remains conservative and stable. The gain in computation time is of order 2^{n_0} if the number of small cells is small.

5. An industrial application

5.1. **Description.** The industrial system that we wish to simulate is a gas generator whose geometry and working order are indicated in Figure 5.1. The gas generator is made of a combustion chamber (top), a cooling chamber (middle part) and an evacuation pipe (bottom, not represented). Only the working order in the cooling chamber will be numerically simulated.

The cooling chamber and the evacuation pipe are separated by a metallic membrane. This membrane can withstand a pressure of 40 bar. The cooling chamber is around 1 m high, it is itself split into several chambers: a central one and a secondary one which communicate through an intermediate chamber and two series of holes.

At time $t = 0$ ms, the cooling chamber is filled with motionless air and water at a pressure of 5 bar. Gas at high pressure ($\sim$ 100 bar) and high temperature ($\sim$ 2500 K) are then produced in the combustion chamber. They rush into the cooling chamber and impact on the water surface causing a shock wave to propagate in the water. When it reaches the bottom membrane, it smashes it. A part of the water is then drained in the evacuation pipe, the rest of the water is transferred into the secondary chamber where it is finally re-injected through very small holes in the draining pipe and mixed with the gas still rushing from the combustion chamber. The entire process, from the beginning of combustion to the beginning

of the liquid re-injection has an approximate duration of 50 ms. This justifies the fact that we neglect vaporization. Of course, for longer simulations, vaporization should be taken into account.

As one can note in Figure 5.1, the real geometry of the cooling chamber is not axisymmetrical due to the presence of re-injection holes near the draining pipe and connection holes between the several chambers. For the simulation we thus replace these holes by slits of equivalent area. The simplified axisymmetrical geometry is represented in Figure 5.2. Here we plot the density. Red corresponds to density values of the liquid (~ 1000 kg/m^3) whereas black corresponds to density values of the gas (~ 10 kg/m^3).

5.2. **Results.** A part of the mesh is represented in Figure 5.3. It appears that very small cells are necessary in the injection slits. The CFL stability condition is thus very restrictive on these cells. In order to avoid a overly long computation we use the algorithm described in §4.3. With this technique it is possible to perform a 50 ms simulation in 5 hours CPU on an 1.4 GHz computer. It should be noted that the exact Riemann solver requires at most 5 Newton iterations for convergence to within $10^{-10}p_0$ where p_0 is the atmospheric pressure. Most of the zones in the fluid flow do not require as many iterations - 2 or 3 only. In conclusion, the classical Godunov scheme is not as expensive as is so often proclaimed in the literature.

We then run the scheme presented in §4.1 and §4.2. Gravity is neglected. The boundary conditions and initial conditions are depicted in Figure 5.2. The boundary conditions are imposed according to the technique described in §4.2:

- At the top entrance of the cooling chamber, which corresponds to the exit of the combustion chamber, we impose pressure $p(t)$ and density $\rho(t)$. The time evolution of these quantities is determined by experimental measurements. The pressure increases from 10 to 120 bar in several milliseconds. We observe that the speed increases from 10 to 700 m/s. The flow thus remains subsonic.
- At the bottom exit, the boundary condition is, at first, a solid wall condition. When the pressure reaches 40 bar (this occurs around 6 ms), the boundary condition is changed into an outflow condition. We then impose an outside pressure of 5 bar. The pressure then drops progressively from 40 to 5 bar, and the velocity increases from 0 to 1500 m/s. The flow is thus supersonic at the end of the computation.

Then, in Figures 5.4, 5.5 and 5.6 iso-densities for several instants are plotted. We can point out the following:

- At 10 ms, the gas begins to push the water. The free surface is slightly deformed. We observe a smoothing of the density profiles due to the numerical diffusion of the interface. But despite the first order scheme (and thanks to a quite fine mesh..)., the interface is easily recognized.
- The instant 15 ms is after the bursting of the membrane. We can see that the central part of the water in the cooling chamber has been drained into the evacuation pipe.
- At instants 20 ms and 25 ms, water has already entered the secondary chamber, forming a jet against its boundary. The jet is numerically diffused but still visible.
- At instant 50 ms, the jet has impacted on the free surface in the secondary chamber. We observe that the re-injection has started (small jet at the bottom).

FIGURE 5.1. Gas generator

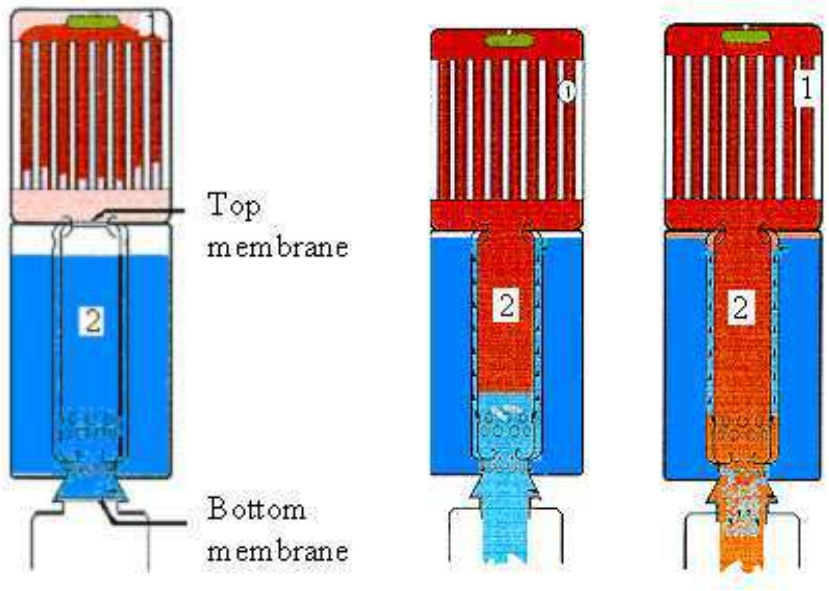

(a) gas-generator (start) (b) gas-generator (middle) (c) gas-generator (end)

- In Figure 5.4, we plot pressure in order to demonstrate the appearance of negative values of the pressure. These negative values appear in the bottom nozzle where a strong drop of pressure is probably triggering cavitation.

Measurements on a real gas generator were performed at the "Direction des Constructions Navales" (DCN) in Toulon (France). Excellent agreement is observed in the central part of the cooling chamber. For example, the bursting time of the separating membrane is predicted with an error of a few percent. More precise comparisons with experiments have now to be performed in the secondary chambers.

6. Conclusion

In this paper we have first recalled basic facts on compressible multifluid flows. We have also carefully described the spurious pressure oscillations phenomenon that arises in any conservative Godunov scheme applied to multifluid flows.

We focused on two remedies to suppress these oscillations. The first fix has been proposed by Saurel and Abgrall in [24]. It is based on a nonconservative transport of the pressure law coefficients and works only for a stiffened gas pressure law. The second fix is, to our knowledge, new and is based on a Lagrange plus projection scheme. In the projection step we project the pressure instead of the pressure law coefficients. The resulting scheme is more diffusive than the Saurel-Abgrall scheme but also more general (it works for any pressure law).

Because in our application the stiffened gas law is sufficient we decided to exploit the Saurel-Abgrall scheme in a 2D axisymmetrical and complex geometry. We had then to deal with some practical problems: negative pressures, axisymmetry, unstructured meshes, boundary conditions, multi time steps.

FIGURE 5.2. Boundaries

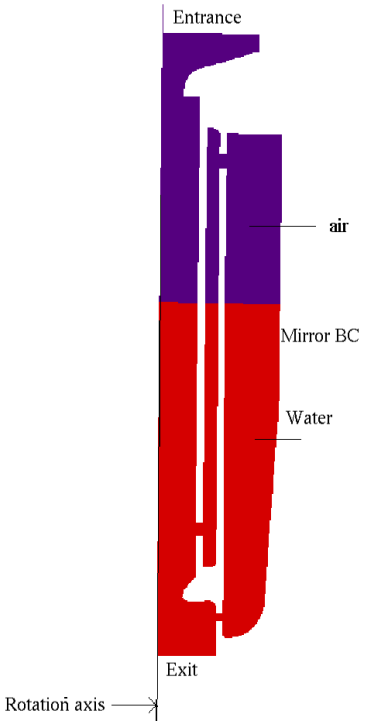

(a) axisymmetrical geometry and boundaries

FIGURE 5.3. Mesh

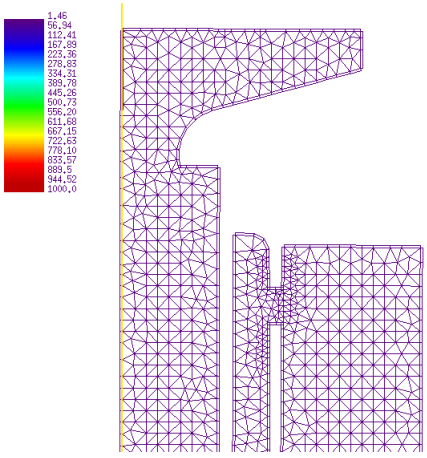

(a) Mesh (partial view)

After having solved these problems, we were in a situation to present a useful industrial numerical simulation.

Future studies could now follow several directions:

FIGURE 5.4. Cavitation

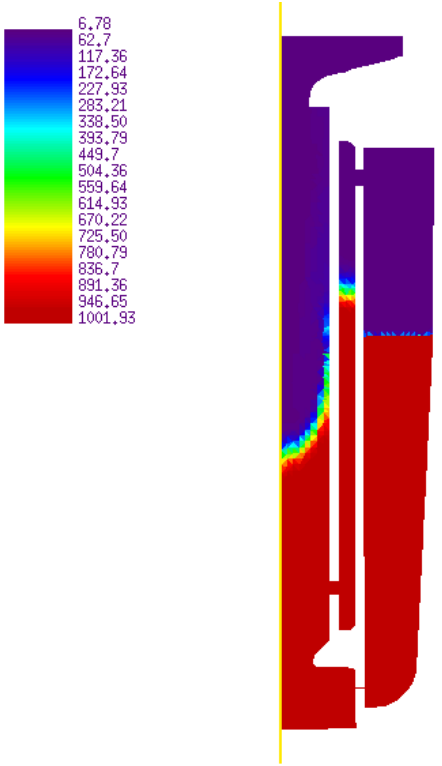

(a) density (kg/m^3) at 10 ms

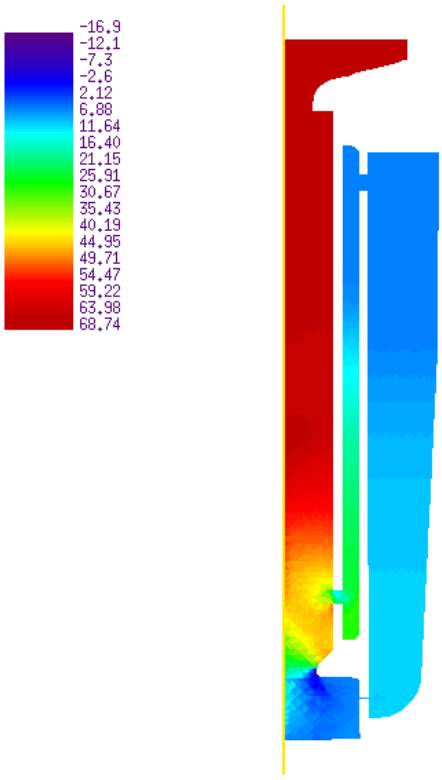

(b) pressure (bar) at 10 ms

FIGURE 5.5. Density plots (kg/m^3)

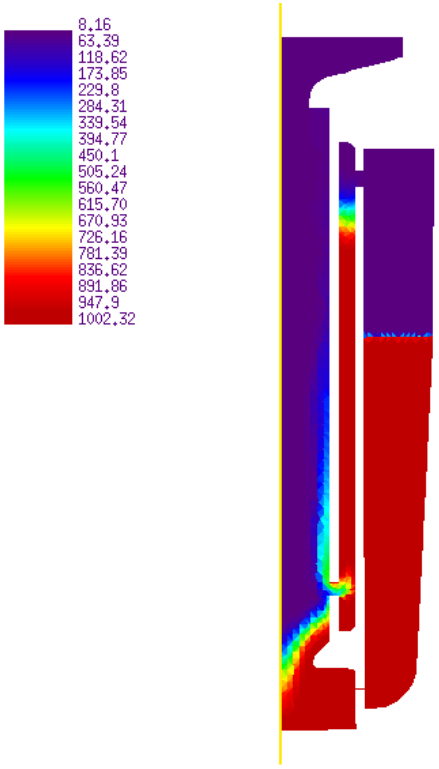

(a) density at 15 ms

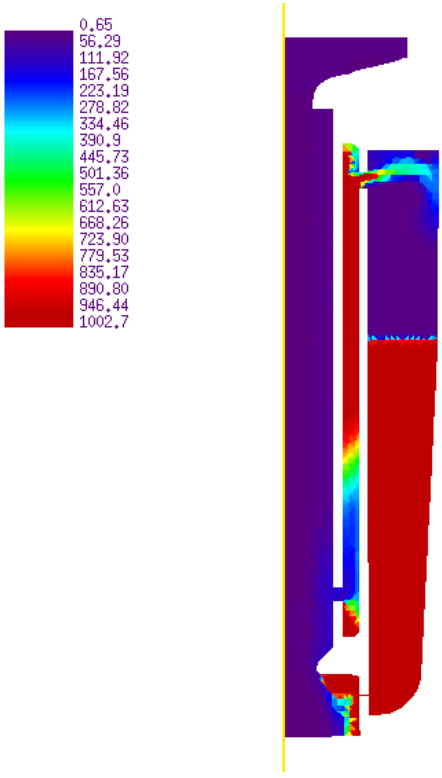

(b) density at 20 ms

FIGURE 5.6. Density plots (kg/m^3)

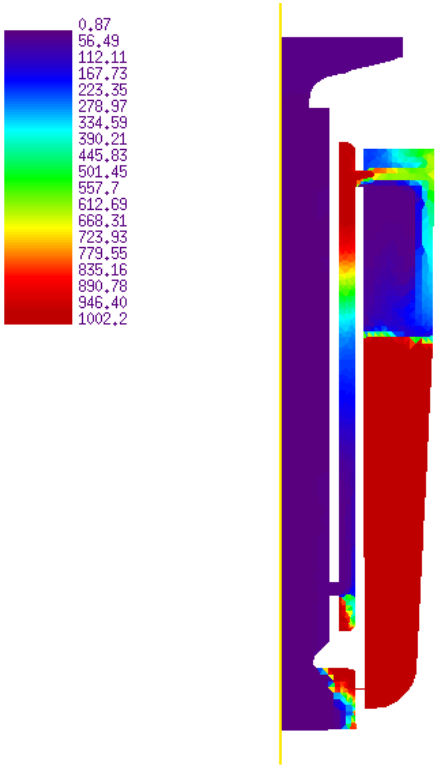

(a) density at 25 ms

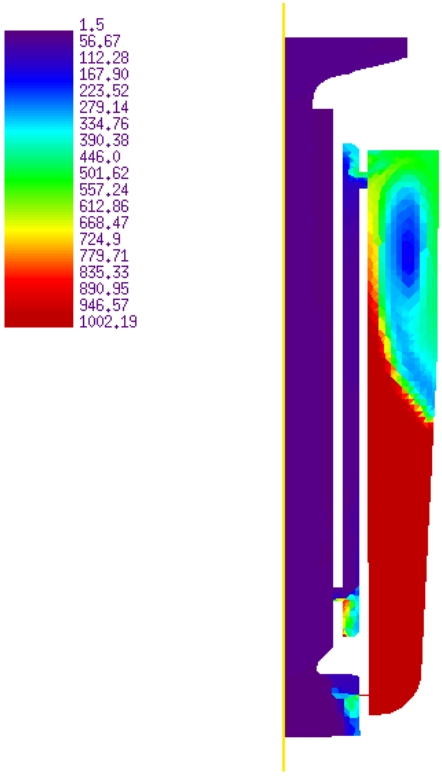

(b) density at 50 ms

- The scheme should be extended to second order. We have not done it because in axisymmetrical cases, the classical second order extensions (as the MUSCL method of Van Leer [26]) are surprisingly not straightforward.
- The second important aspect is to be able to deal with true cavitation, i.e. the vaporization of the liquid in a metastable state. Some progress has been obtained in the case of a liquid-vapor flow in [16]. The case of the three-phase flow with air, liquid and vapor is being studied. Some preliminary results can be found in [4].

7. Appendix

7.1. **Entropy and hyperbolicity.** We study here the hyperbolicity of (2.9), (2.1). For this purpose, it is classical to introduce the specific entropy

$$s^0 = \frac{p+\pi}{\rho^\gamma} = s^0(W).$$

A simple computation shows that if W is a regular solution of (2.1), (2.9), then s^0 satisfies the advection equation

$$s^0_t + u s^0_x = 0.$$

Thus, for any function g of s^0, γ and π an additional conservation law is satisfied by $\rho g(s^0,\gamma,\pi)$

$$(\rho g(s^0,\gamma,\pi))_t + (\rho u g(s^0,\gamma,\pi))_x = 0.$$

If $W \to S(W) = \rho g(s^0,\gamma,\pi)$ is convex, we get in this way all the Lax entropies of system (2.9), (2.1). For a proof of this result, we refer to the review paper of [15]. According to Mock's theorem [21] the convexity of S would then imply hyperbolicity. Here, we prefer to carry out a more direct calculation. Always for regular solutions, we set

$$Y = \begin{pmatrix} \rho \\ u \\ s^0 \\ \gamma \\ \pi \end{pmatrix}.$$

We then have

$$Y_t + B(Y) Y_x = 0,$$

with

$$B(Y) = \begin{pmatrix} u & \rho & 0 & 0 & 0 \\ \gamma\frac{p+\pi}{\rho^2} & u & \rho^{\gamma-1} & \frac{(p+\pi)\ln(\rho)}{\rho} & -\frac{1}{\rho} \\ 0 & 0 & u & 0 & 0 \\ 0 & 0 & 0 & u & 0 \\ 0 & 0 & 0 & 0 & u \end{pmatrix}.$$

The eigenvalues of B are $(u-c, u, u, u, u+c)$ with $c^2 = \gamma\frac{p+\pi}{\rho}$. Thus, if $\rho > 0$, the system is hyperbolic if and only if

$$p + \pi \geq 0.$$

Remark 7.1. When p tends to $-\pi$ keeping the specific entropy constant, which is the case in a rarefaction wave, we get:

$$\rho = C\ (p+\pi)^{1/\gamma} \to 0.$$

Thus, the limiting case $p = -\pi$ corresponds to a zero density $\rho = 0$. This means that, in a liquid, vacuum corresponds to a negative value of the pressure.

7.2. **Global resolution of the Riemann problem.** As in the case of gas dynamics for one fluid, the fields 1 and 3, which correspond to the eigenvalues $u-c$ and $u+c$ are genuinely non-linear whereas the field 2 corresponding to the multiple eigenvalue u is linearly degenerate (contact discontinuity).

At present, we have written several forms (conservative or not) for the convection equations. All these forms are formally equivalent. It is important to verify that they are correct also for discontinuous solutions.

Let us consider a discontinuity propagating with velocity σ. Indexes (a) and (b) will be relative to the two sides of the discontinuity. Rankine-Hugoniot relations read, in this case

$$\sigma(W_a - W_b) = F(W_a) - F(W_b).$$

Introducing the relative velocity to the discontinuity and the specific volume

$$v = u - \sigma, \qquad \tau = \frac{1}{\rho},$$

the jump relations become

$$\begin{aligned} M = \rho_a v_a &= \rho_b v_b, \\ \rho_a v_a^2 + p_a &= \rho_b v_b^2 + p_b, \\ (\rho_a(\varepsilon_a + \frac{v_a^2}{2} + p_a)v_a &= (\rho_b(\varepsilon_b + \frac{v_b^2}{2}) + p_b)v_b, \\ M\gamma_a &= M\gamma_b, \\ M\pi_a &= M\pi_b. \end{aligned}$$

The last two relations implie that γ and π can jump only at the contact discontinuity (when $M = 0$). On the other hand, a simple computation shows that γ and π are Riemann invariants for the fields 1 and 3.

Remark 7.2. These two properties imply that in genuinely non-linear fields the coefficients γ and π are constant. Outside the contact discontinuity, the computations are thus identical to the case of a single fluid. These classical computations can be found for example in the book of Godlewski and Raviart [13]. They are briefly sketched below.

Remark 7.3. We have also given a sense to the nonconservative products in the last two transport equations in (2.16) because u and the pressure law coefficients cannot present a simultaneous jump.

Solving the Riemann problem means finding the weak entropy solution of

$$\begin{gathered} W_t + F(W)_x = 0, \\ W(0,x) = \begin{cases} W_l \text{ if } x < 0, \\ W_r \text{ if } x > 0. \end{cases} \end{gathered}$$

This solution is supposed to be self-similar

$$W(t,x) = R\left(\frac{x}{t}, W_l, W_r\right).$$

It is made up of constant states separated by shock waves, rarefaction waves or a contact discontinuity. It is thus of the form

$$R(\xi, W_l, W_r) = \begin{cases} W_l & \text{if} \quad \xi < \lambda_1^-, \\ W_I & \text{if} \quad \lambda_1^+ < \xi < \lambda_2, \\ W_{II} & \text{if} \quad \lambda_2 < \xi < \lambda_3^-, \\ W_r & \text{if} \quad \lambda_3^+ < \xi, \end{cases}$$

where the unknowns are W_I, W_{II} and the velocities λ_2, $\lambda_i^\pm$, $i = 1, 3$ which satisfy $\lambda_1^- \le \lambda_1^+ < \lambda_2 < \lambda_3^- \le \lambda_3^+$.

Furthermore, if $\lambda_i^- < \lambda_i^+$ (resp. if $\lambda_i^- = \lambda_i^+$) then the i-wave is a rarefaction wave (resp. a shock of velocity $\sigma = \lambda_i^- = \lambda_i^+$). When the i-wave is a rarefaction, the computation of $W = R(\xi, W_l, W_r)$, for $\lambda_i^- < \xi < \lambda_i^+$ is classically carried out by expressing that the three Riemann invariants are constant in the i-rarefaction (see [13]).

On the other hand, we have $p_I = p_{II} = p^\star$. If no vacuum occurs, we can also write $u_I = u_{II} = u^\star$. Moreover, from remark 7.2, we have that $\gamma_I = \gamma_l$, $\gamma_{II} = \gamma_r$, $\pi_I = \pi_l$, $\pi_{II} = \pi_r$. It is then classical to compute the 1- and 3-waves from the pressure $p^\star$ common to the two intermediate states W_I et W_{II}. For this purpose, we introduce the functions

$$h_a(p^\star) = \tau_a \frac{(\gamma_a+1)(p_a+\pi_a)+(\gamma_a-1)(p^\star+\pi_a)}{(\gamma_a+1)(p^\star+\pi_a)+(\gamma_a-1)(p_a+\pi_a)}, \quad a = l \text{ or } r,$$

$$\Phi_a(p^\star) = \sqrt{(p^\star - p_a)(\tau_a - h_a(p^\star))},$$

$$g_a(p^\star) = \tau_a \left(\frac{p_a+\pi_a}{p^\star+\pi_a}\right)^{1/\gamma_a},$$

$$\Psi_a(p^\star) = \frac{2}{\gamma_a - 1}(\tau_a\gamma_a(p_a+\pi_a))^{1/2}\left((\frac{p^\star+\pi_a}{p_a+\pi_a})^{\frac{\gamma_a-1}{2\gamma_a}} - 1\right),$$

$$X_a(p^\star) = \begin{cases} \Phi_a(p^\star) & \text{if} \quad p^\star > p_a, \\ \Psi_a(p^\star) & \text{if} \quad p^\star < p_a, \end{cases}$$

$$H_a(p^\star) = \begin{cases} h_a(p^\star) & \text{if} \quad p^\star > p_a, \\ g_a(p^\star) & \text{if} \quad p^\star < p_a. \end{cases}$$

We thus get

$$u_I = u_l - X_l(p^\star),$$

$$u_{II} = u_r + X_r(p^\star),$$

$$\tau_I = H_l(p^\star),$$

$$\tau_{II} = H_r(p^\star),$$

and the Riemann problem is solved when $p^\star$ is known.

If no vacuum region appears, the following theorem holds.

Theorem 7.4. *Let $p_0 = \min(\pi_l, \pi_r)$. If*

$$u_r - u_l \leq -\left(X_l(-p_0) + X_r(-p_0)\right), \tag{7.1}$$

then the Riemann problem has a unique solution. The pressure $p^\star \geq -p_0$ is the unique solution of

$$u_l - X_l(p^\star) = u_r + X_r(p^\star).$$

This result is quite similar to the case of the Riemann problem for a single fluid. For the proof we refer (for example) to [14], [13].

When inequality (7.1) is not true, a vacuum has to be introduced. This vacuum region appears in the fluid whose coefficient π is the smallest.

Theorem 7.5. *If*

$$u_r - u_l > -\left(X_l(-p_0) + X_r(-p_0)\right),$$

the Riemann problem has still an entropy solution. For example, if $p_0 = \pi_l$, then we have $p^\star = -p_0$, $\rho_I = 0$, $u^\star = u_{II} = u_r + X_r(p^\star)$. $u_I = u_l - X_l(p^\star)$, and, in general $u_I \neq u_{II}$.

Proof. Suppose that $p_0 = \min(\pi_l, \pi_r) = \pi_l$. In the two open sets $x < u^\star t$ and $x > u^\star t$, the computation of the 1- and 3-wave curves is identical to the mono-fluid case. Thus, $W(t,x)$ is indeed an entropy solution of the Riemann problem in these two open sets. It is then sufficient to verify that, at the contact discontinuity $x/t = u^\star$, Rankine-Hugoniot jump relations are satisfied, together with the entropy condition. The discontinuity velocity is $\sigma = u^\star$. We thus have $v_{II} = u^\star - \sigma = 0$. Mass conservation $\rho_I v_I = 0 = \rho_{II} v_{II}$ is then satisfied. In the same way, $\rho_I v_I^2 + p^\star = p^\star = \rho_{II} v_{II}^2 + p^\star$. The jump relation for the conservation of $\rho\varphi$ is also satisfied: $\rho_I v_I \varphi_I = 0 = \rho_{II} v_{II} \varphi_{II}$. For the energy jump relation, we use the fact that the 1-wave is necessarily a rarefaction because $p^\star = -p_0 \leq p_l$. However, in a rarefaction, when $p \to -\pi$, then $\rho\varepsilon + \pi \to 0$ (see remark 7.1) and we have $(\rho_I \varepsilon_I + p^\star) v_I + \rho_I \frac{v_I^3}{2} = 0 = (\rho_{II}\varepsilon_{II} + p^\star) v_{II} + \rho_{II} \frac{v_{II}^3}{2}$. Finally, the entropy inequality (which degenerates to an equality) is also satisfied: $\rho_I v_I s_I = 0 = \rho_{II} v_{II} s_{II}$. □

References

[1] R. Abgrall. Generalisation of the roe scheme for the computation of mixture of perfect gases. *Recherche Aérospatiale*, 6:31–43, 1988.

[2] R. Abgrall. How to prevent pressure oscillations in multicomponent flow calculations: a quasi-conservative approach. *J. Comput. Phys.*, 125(1):150–160, 1996.

[3] R. Abgrall and S. Karni. Computations of compressible multifluids. *Journal of Computational Physics*, 169(2):594–623, 2001.

[4] T. Barberon. *Modélisation mathématique et numérique de la cavitation dans les écoulements multiphasiques compressibles*. PhD thesis, Université de Toulon, 2002.

[5] C. Berthon and B. Nkonga. Behavior of the finite volumes schemes in material and numerical interfaces. In *Finite Volumes for Complex Applications III (Porquerolles, 2002)*, pages 139–146. Hermes Penton Ltd, London, 2002.

[6] A. Chalabi and J.-P. Vila. Operator splitting, fractional steps method and entropy condition. In *Third International Conference on Hyperbolic Problems, Vol. I, II (Uppsala, 1990)*, pages 226–240. Studentlitteratur, Lund, 1991.

[7] J. P. Cocchi and R. Saurel. A Riemann problem based method for the resolution of compressible multimaterial flows. *Journal of Computational Physics*, 137(2):265–298, 1997.

[8] F. Dubois. Partial riemann problem, boundary conditions and gas dynamics. In *Absorbing Boundaries and Layers, Domain Decomposition Methods. Applications to Large Scale Computations, Loïc Tourrette and Laurence Halpern, eds.*, pages 16–77. Nova Science Publishers, Inc., New York, 2001.

[9] F. Dubois and P. LeFloch. Boundary conditions for nonlinear hyperbolic systems of conservation laws. *J. Differential Equations*, 71(1):93–122, 1988.

[10] R. P. Fedkiw, T. Aslam, B. Merriman, and S. Osher. A non-oscillatory Eulerian approach to interfaces in multimaterial flows (the ghost fluid method). *J. Comput. Phys.*, 152(2):457–492, 1999.

[11] J. P. Franc and *al. La Cavitation: Mécanismes Physiques et Aspects Industriels*. Presses Universitaires de Grenoble, 1995.

[12] T. Gallouët, J. M. Hérard, and Seguin N. A hybrid scheme to compute contact discontinuities in one-dimensional euler systems. *M2AN*, 36(6):1133–1159, 2003.

[13] E. Godlewski and P. A. Raviart. *Numerical approximation of hyperbolic systems of conservation laws*. Springer, 1996.

[14] S. Godounov, A. Zabrodine, M. Ivanov, A. Kraĭko, and G. Prokopov. *Résolution numérique des problèmes multidimensionnels de la dynamique des gaz*. "Mir", Moscow, 1979. Translated from the Russian by Valéri Platonov.

[15] A. Harten, P. D. Lax, C. D. Levermore, and W. J. Morokoff. Convex entropies and hyperbolicity for general Euler equations. *SIAM J. Numer. Anal.*, 35(6):2117–2127, 1998.

[16] P. Helluy and T. Barberon. Finite volume simulations of cavitating flows. In *Finite Volumes for Complex Applications III (Porquerolles, 2002)*, pages 455–462. Hermes Penton Ltd, London, 2002.

[17] T. Y. Hou and P. G. LeFloch. Why nonconservative schemes converge to wrong solutions: error analysis. *Math. Comp.*, 62(206):497–530, 1994.

[18] S. Karni. Multicomponent flow calculations by a consistent primitive algorithm. *Journal of Computational Physics*, n 47:1115–1145, 1994.

[19] S. Karni. Hybrid multifluid algorithms. *SIAM J. Sci. Comput.*, 17(5):1019–1039, 1996.

[20] P. Kuszla and V. Daru. Numerical simulation of high-speed liquid jets. In *Computational mechanics (Buenos Aires, 1998)*. Centro Internac. Métodos Numér. Ing., Barcelona, 1998.
[21] M. S. Mock. Systems of conservation laws of mixed type. *J. Differential Equations*, 37(1):70–88, 1980.
[22] W. Mulder, S. Osher, and J. A. Sethian. Computing interface motion in compressible gas dynamics. *J. Comput. Phys.*, 100(2):209–228, 1992.
[23] S. Rouy. *Modélisation mathématique et numérique d'écoulements diphasiques compressibles*. PhD thesis, Université de Toulon, December 2000.
[24] R. Saurel and R. Abgrall. A simple method for compressible multifluid flows. *SIAM J. Sci. Comput.*, 21(3):1115–1145, 1999.
[25] R. Saurel, J.P. Cocchi, and P.B. Butler. A numerical study of cavitation in the wake of a hypervelocity underwater projectile. *AIAA Journal of Propulsion and Power*, 15(4):513–522, 1999.
[26] B. Van Leer. Towards the ultimate conservative difference scheme. a second order sequel to the godunov's method. *Journal of Computational Physics*, 32:101–136, 1979.